Optimization of Obstacle Detection for Small UAVs

Pedro Serrano
pedro.miguel.silva.serrano@tecnico.ulisboa.pt

Instituto Superior Técnico, Universidade de Lisboa, Portugal

June 2022

Abstract

The UAV market grows every year and in order to keep this, it is required a large investment in Sense and Avoid systems. With this in mind, the thesis is centred on this type of systems with special focus on the detection phase in small fixed-wing UAVs. Firstly, a presentation of the various types of available sensors and avoidance algorithms is made culminating with a list of the most suitable sensors for this type of work and a background explanation on the Potential fields method that will be used as the avoidance algorithm. Next, parameters are defined to characterize the sensing systems and then tested in simulated obstacle avoidance missions. At the end of these simulations, several conclusions were drawn on the influence of the parameters in the overall performance of the system. The work continues with a presentation of the hardware and software required to implement a Sense and Avoid system. After the sensors and controller have been chosen, a schematic is drawn up with all the necessary devices and the connections between them. Furthermore, the flight controller firmware and the ground control station software are chosen taking into account their specifications. Next, the work proceeds to the elaboration of experiments with the sensors, obtaining real information about their capabilities such as maximum range, average error of the measurements, etc. Finally, a simple sense and avoid system is implemented in a small rover in order to perform experiences that can evaluate the capabilities of the sense and avoid system.

Keywords: UAVs, Sense and Avoid, Potential Fields, Parameters, Rover

1. Introduction

The history of UAVs is highly intertwined with the wars of the last century. Since the appearance of their first models during the First World War, several subsequent armed conflicts have driven the development of this technology up to the present day [14]. As time went by, the full potential of this type of vehicle began to be applied to new markets, making UAVs an extremely desirable product in industries such as entertainment, precision agriculture, transport or even inventive projects such as FireFront [9]. In light of this reality, an increase of over 13 thousand million dollars is expected in the production of civil UAVs between 2020 and 2029 [13].

Classification of UAVs becomes very important in an era of such rapid growth, as different types of UAVs will have widely varying uses and possibly different regulations. Using the classification system presented in [12], one can limit this study to fixed wing mini UAVs due to their significant market share, versatility and low cost [6]. Figure 1 shows the AR4, which is a UAV model produced by the Portuguese company Tekever and which illustrates quite well the chosen UAV category. This aircraft is characterised by its MTOW of 4 kg, an endurance of 2 h and a wingspan and length of 2.1 m and 1.35 m respectively.

Figure 1: AR4 by Tekever[4]

For products like this one from tekever to emerge in increasing numbers, there is a long way to go to overcome various technical and legal barriers. The development of Sense and Avoidance (S&A) systems is one of the most interesting challenges in the UAV market, since it may be the key to a faster integration of UAVs in urban environments. Therefore, the main goal of this work is to contribute to a study on this type of systems, with special focus on the detection phase.

2. Sense and Avoid Systems

Sense and Avoidance systems usually have an architecture like the one shown in Figure 2. The process begins with the sensing stage, where one or several sensors installed in the system gather external information. Hereupon, the avoidance stage must evaluate the situation and, if needed, plan an alternative path to avoid a collision. Hereupon, a flight controller must be capable to put the UAV following this alternative path.

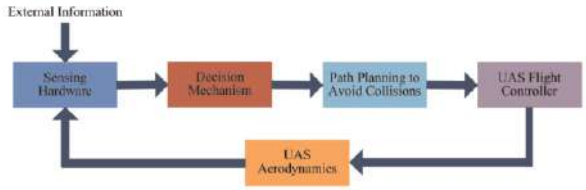

Figure 2: Architecture of an S&A system [15]

2.1. Sensing Stage

As previously mentioned, the sensing stage is the first major task of an S&A System. In order to optimize the process, it will be necessary to select the sensors according to the mission at hand. The best way to do that is by exploring all the possible solutions in the market. Cooperative and non-cooperative sensors appear as the two possible options to target.

Non cooperative sensors were immediately chosen as they do not required the same technology to be installed on the intruder side. Inside this category, active sensors were selected as they do not require an external signal.

The most common types of non-cooperative active models are RADARs, Ultrasonic Sensors and Laser Rangefinders. All of them can output a distance to an object by emitting a signal and then measuring the time it took until a reflection was received. As the velocity that their specific signal travels is known, a distance to the reflection surface can be obtained. The difference between them is the signal they used. While RADARs and laser rangefinders use light (radio waves and infrared respectively), ultrasonic sensors use sound waves. The characteristics of each one of these signals can determine the sensors' capabilities or limitations. For example RADARs can be extremely efficient with presence of clouds, fogs or snow in the sky due to the greater wavelength of radio waves. On the other hand, infrared waves have shorter wavelengths, making laser rangefinders a better option to detect smaller targets.

2.2. Avoiding Stage

The avoiding stage is responsible to generate a new path capable of deviating the aircraft from the intruder and to return to the previously define trajectory afterwards.

When addressing the topic of avoidance algorithms several options can appear such as geometric approaches, graph search algorithms or the potentials fields method. Potential field algorithm was chosen based in [7], and will be covered in detail.

2.2.1 Potential Fields Method

This method is based on Coulomb's law. The idea is to consider every intruder as a repulsive charge and the next waypoint on the path as an attractive charge [8]. The summation of these charges should return the safest direction to follow at each instance of time.

Safety zones This algorithm was previously implemented with safety zones (see Figure 3) associated to each obstacle [7][6]. In these implementations, all objects were defined as spheres and each one has a collision radius associated ($\boldsymbol{R_C}$), which is equal to the obstacle radius. A **collision** is said to occur when an UAV passes through this radius. The safety radius ($\boldsymbol{R_S}$) has a similar definition but accounts for some uncertainties. The action radius ($\boldsymbol{R_a}$) is the distance from which the replanned path starts to depart from the original path given by the global planner while $\boldsymbol{R_d}$ is the detection radius provided by the distance sensor.

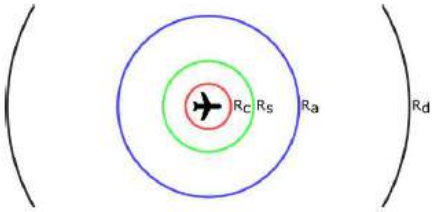

Figure 3: Safety zones [6]

Attractive Field In the most common cases, the UAV needs to follow a well determined path. The idea is to sum up two components for the attractive field as seen in equation (1). The first one pointing from the UAV position, P_{UAV} to the closest point on the path, P_{close} and the last one pointing from P_{close} to the next waypoint on the path, P_{next}. There is also a parameter, α_{PF} that adjusts the relevance of each term. When $\alpha_{PF}$is close to 1 the algorithm is valuing more the approximation to the path. On the other hand, when α_{PF} is close to 0, the algorithm is preferring to follow the path direction [7]. Figure 4 shows an example of an attractive field defined by equation 1, where these two components can be identified.

$$\mathbf{f}_{at} = \alpha_{PF} \frac{P_{close} - P_{UAV}}{\|P_{close} - P_{UAV}\|} + \alpha_{PF} \frac{P_{next} - P_{close}}{\|P_{next} - P_{close}\|} \quad (1)$$

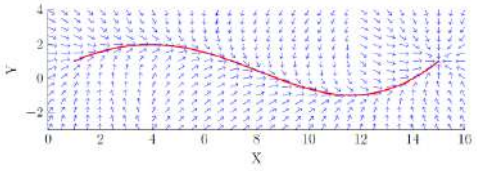

Figure 4: Attractive field with two components (α_{PF}=0.5)[7]

Repulsive Field The repulsive field is similar to the attractive one. However, there are new variables to be dealt with, specially distance. For this reason, $\boldsymbol{d_0}$ is used representing a vector pointing from the object centre to the UAV. In addiction to this variable there is also a swirling unit vector,

$$\boldsymbol{s} = \frac{\hat{\boldsymbol{k}} \times \boldsymbol{d_0}}{\|\boldsymbol{d_0}\|}, \quad (2)$$

where $\hat{\boldsymbol{k}}$ is the z axis unit vector. The idea is to define this potential function according to the barriers exposed in Figure 3 resulting in a repulsive field like the one represented in Figure 5. Inside the collision area, the potential function will be infinite with $\boldsymbol{d_0}$ orientation . Within the close call region, the potential will be at its maximum value, S_{max} but the direction will be given by $\boldsymbol{s}$ or its inverse. For the action area the potential is almost the same, but it decreases linearly from S_{max} to zero. Finally, outside the action area the repulsive field will be null, as expected. Each one of this cases is described in this specific order in (3).

$$\begin{cases} \infty \dfrac{\boldsymbol{d_0}}{\|\boldsymbol{d_0}\|} & \text{, if } \|\boldsymbol{d_0}\| \leq R_c \\ S_{max}\boldsymbol{s} & \text{, if } R_c < \|\boldsymbol{d_0}\| \leq R_s \\ S_{max} \dfrac{R_a - \|d_0\|}{R_a - R_s} \boldsymbol{s} & \text{, if } R_s < \|\boldsymbol{d_0}\| \leq R_a \\ 0 & \text{, if } \|\boldsymbol{d_0}\| \geq R_a \vee \theta \leq \theta_{cut-off} \end{cases} \quad (3)$$

This approach with a swirling potential in safety and action areas prevents the UAV from an irregular motion around the object but at the same time can trap it in a continuously circular motion. This problem is solved considering an angle, θ, between the desired direction of motion ($\boldsymbol{m}$) and $\boldsymbol{d_0}$ given by

$$\theta = \arccos \frac{\boldsymbol{m} \cdot \boldsymbol{d_0}}{\|\boldsymbol{d_0}\|\|\boldsymbol{m}\|}. \quad (4)$$

When θ reaches a fixed value, $\theta_{cut-off}$, the potential function returns to 0.

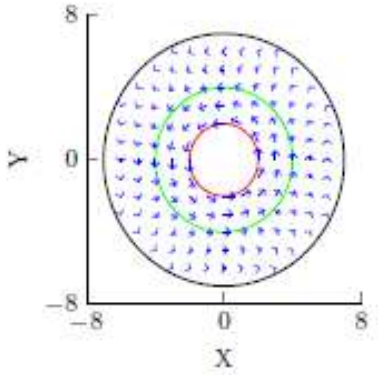

Figure 5: Repulsive field [6]

3. Sensor Parametric Studies

In order to optimize a sense and avoidance system, selecting a the right configuration of sensors is crucial. With that in mind, a set of MATLAB simulations were performed, in order to understand which variables affect the overall performance of an S&A system. These simulations were restricted to the sensors available for future hardware implementation: Laser rangefinders and ultrasonic sensors.

3.1. UAV model

Using pre developed work in [7], a simple head on collision was simulated where both UAV and obstacle are moving at the same speed. The idea is to evaluate how much turning speed is required to avoid the obstacle for different values of $\boldsymbol{R_a}$. Results may be seen in Figure 6 where a red line is marking the maximum turning speed, in order to avoid a load factor greater than 4g that could potentially damage the UAV structure.

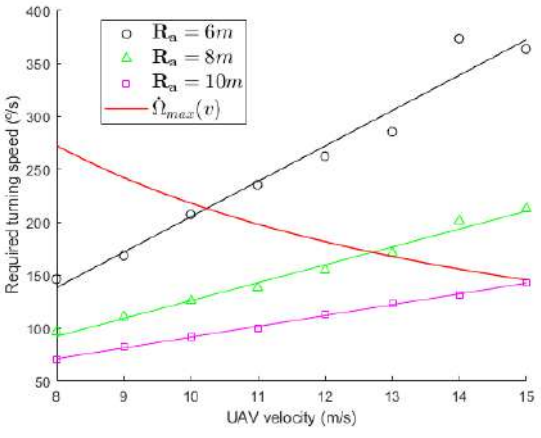

Figure 6: Turning rate required to avoid obstacle safely for different velocities

Results show that it is important to have a sensor with at least 10 m, otherwise there is no avoidance

system that could avoid a crash without risking the UAV structure. Nevertheless, critical situations like this are not that common and sensors with less than 10 m range can still be useful. For future simulations, the maximum turning speed will be always locked to the red function illustrated in Figure 6.

3.2. Numerical Model

In order to evaluate sensor configurations, several steps must be executed as shown in Figure 7. The idea is generate scenarios with static and moving obstacles in random positions and trajectories. For each scenario created, a simulation is performed with no sensors. The first 50 scenarios that lead to collisions/close calls are chosen to future tests. Hereupon, the sensor parameters of the sensor at hand are varied, and for each iteration an objective function is calculated in order to quantify the systems performance.

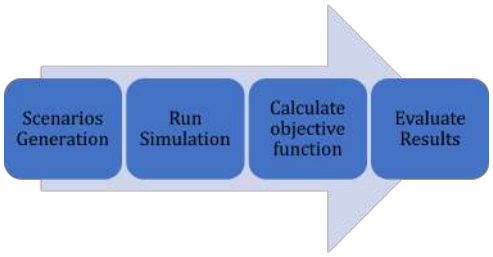

Figure 7: Sensor studies Steps

Objective function In order to evaluate the sensing system in a more adequate way, it was used an objective function, f, just like in [6], which is incorporated in the simulation code. By the end of all simulations, this objective function will assign a value to a specific set of parameters represented by $\boldsymbol{y}$, which include the following parameters:

1. Sensor orientation, β
2. Sensor maximum range, $\boldsymbol{R_d}$
3. Beam format - Binary Variable (Narrow or Wide) only used for ultrasonic sensors

The major problem when evaluating the sensing system performance with the metric explained previously is the fact that a close call severity is not objective. The only thing that can be assumed is that the collision risk increases when the UAV gets closer to the collision frontier and, for this reason, each close call must be evaluated independently. Additionally, there is a clear goal in a Sense and Avoidance mission, which is maximizing the minimum distance to all obstacles.

The objective function, f, is modified to incorporate these guidelines, leading to,

$$\begin{cases} f(\mathbf{y}) = g(\mathbf{y}) + p(\mathbf{y}) \\ g(\mathbf{y}) = -\sum_{i=1}^{n} d_{min}(i) \\ p(\mathbf{y}) = \phi \sum_{i=1}^{n} min(max(0, \mathbf{R_S}(i) - d_{min}(i)), \mathbf{R_S}(i) - \mathbf{R_C}(i))^2 \end{cases} \tag{5}$$

where two distinct functions are summed: goal and penalty function ($g(\mathbf{y})$ and $p(\mathbf{y})$). The first one uses d_{min}, which is an $n \times 1$ matrix with n being the total number of obstacles within the simulation and each entry the minimum distance to that specific obstacle during the entire simulation. The goal function $g(\mathbf{y})$ is symmetric to the sum of all d_{min} entries. The penalty function, $p((\mathbf{y})$ adds penalties if the UAV has passed the Close Call or Collision frontiers. These penalties weights follow a linear function just like it is shown in Figure 8 augmenting from zero at the close call frontier to its maximum penalty, $\phi(\mathbf{R_S} - \mathbf{R_C})$, inside all the Collision region. Finally, the parameter ϕ can be adjusted to augment or decrease the penalty function impact on $f(\mathbf{y})$. At the end, the most successful combination of sensor parameters will have the lowest values of $f(\mathbf{y})$.

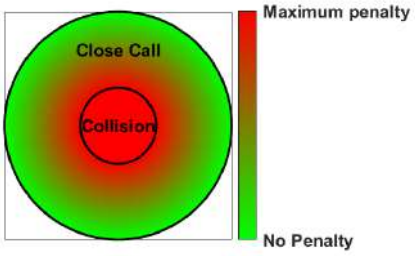

Figure 8: Distribution of the penalties weights

3.3. Laser rangefinder simulations

The results obtained by running the simulations for all combinations of R_d and β are represented in figure 10, while Figure 9 illustrates how the parameters affect the configuration of the system.

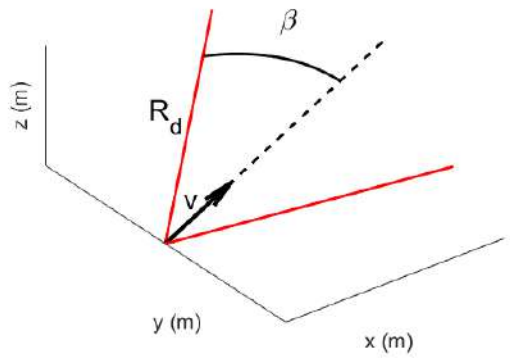

Figure 9: Sensing system model using laser rangefinders

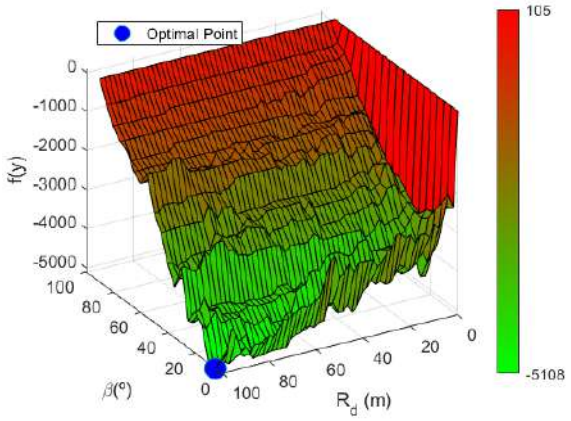

Figure 10: Sensor parameters influence in the objective function

Regarding the sensor orientation β it is pretty clear looking at Figure 10 that the performance of the system suffers a considerable degradation for sensor angular orientations above 20° and this behaviour is consistent independently of whatever $\mathbf{R_d}$ value is being fixed. For $\beta \leq 20°$, it is also clear that the system performance is maximized for $\beta = 5°$, where the optimal point is located. To sum up, the most clear conclusion to take from these results is that the system behaves better when the laser is more aligned with the UAV velocity. This does not mean that $\beta = 0°$ is the best possible orientation because small values of β can also cover all the obstacles present directly in front of the UAV and with the advantage of having 2 lasers working at the same time. This could obviously suffer a dramatic change if, for example, the dimensions of the obstacles were reduced.

Regarding the maximum range $\mathbf{R_d}$, it is not so easy to look at Figure 10 and immediately extract conclusions about some kind of relation between $f(\mathbf{y})$ and $\mathbf{R_d}$, except for the abrupt reduction of the objective function value from $\mathbf{R_d} = 0\,\text{m}$ to the remaining values. Due to this fact, a statistical analysis was performed to understand if there is in fact a relation between augmenting the laser range and the improvement of the sensing system performance. This analysis was then materialized isolating every function of the type $f(\mathbf{R_d}, \beta = \beta_{fixed})$, and performing a linear regression to each one to understand if the resulting slope of this approximation is negative. Figure 11, represents all the slopes obtained for each β_{fixed}. It is important to mention that, all the points with $\mathbf{R_d} = 0\,\text{m}$ were disregarded for this study.

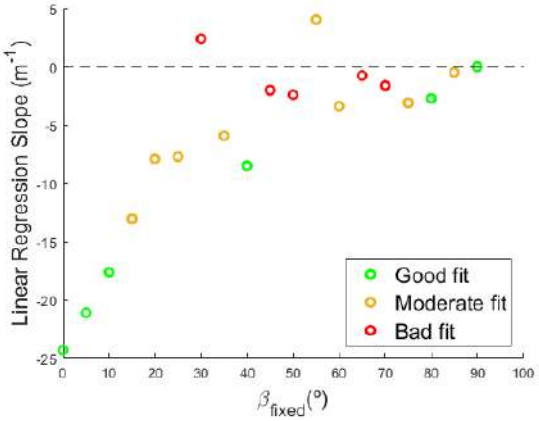

Figure 11: linear Regression for $f(\mathbf{R_d}, \beta = \beta_{fixed})$(laser rangefinder case)

It can be observed in Figure 11 that all the linear regressions made for $\beta_{fixed} \leq 25°$ present a negative slope, suggesting that the sensing system performance tends to augment when the laser range is increased. For $\beta_{fixed} \geq 25°$, this trend almost disappears, suggesting that the bad performance of these configurations is almost determined by their lasers angular orientation with almost no room for improvement.

3.4. Ultrasonic sensor

3.4.1 Model

In contrast to laser sensor, whose model was previously developed in [6] in MATLAB environment, the model for the ultrasonic sensor was not built until now. The idea consists in always verify two conditions:

1. The presence of any spherical surface point within the sonar beam pattern;

2. The perpendicularity of the sound wave direction with its reflection surface.

In order to verify these conditions, the algorithm needs a considerable amount of computing time. To deal with this issue, it was implemented a progressively complex approach that avoids unnecessary blocks of code. At the end of its task, all points of the obstacle's surface that verify those two conditions at the same time are listed and the closest one to the UAV is selected. It is also important to add that the following simulations are going to be repeated for a narrow and a wide beam pattern.

3.4.2 Simulations

The results of these simulations are expressed in Figure 12 where the blue dot represent the optimal parameters. With regard to β, it is obvious looking at Figure 12, that there is a clear minimum at $\beta = 20^{\circ}$ and $\beta = 10^{\circ}$ for the narrow and wide beam patterns respectively and that is valid for any range value. When augmenting these angles, the results deteriorate in both cases, although the wide beam pattern can sustain a reasonable performance until $\beta = 40^{\circ}$.

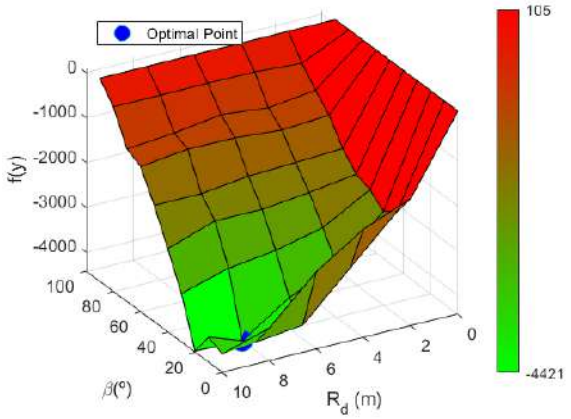

(a) Narrow Beam Pattern

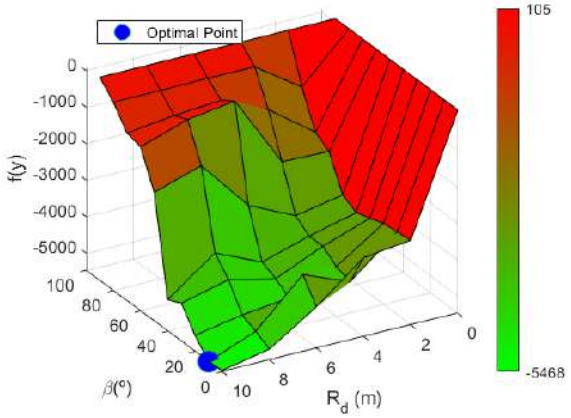

(b) Wide Beam Pattern

Figure 12: Ultrasonic sensor parameters influence in the objective function.

Similarly to what was done with the laser rangefinder studies, a linear regression approach was used to find any possible relations between $\mathbf{R_d}$ and the sensing system performance.

After isolating several functions of the type $f(\mathbf{R_d}, \beta = \beta_{fixed})$ and removing all points with $\mathbf{R_d} = 0\,\mathrm{m}$, the graphics illustrated in Figures 13 and 14 were obtained. In Figure 13a), it can be observed that the great majority of the plotted points correspond to a negative slope, meaning that augmenting $\mathbf{R_d}$ is causing a decrease of the objective function value or, in other words, improving the performance of the sensing system. Additionally, the magnitude of these slopes tends to decrease for larger β_{fixed} values, which leads to the same conclusion extracted from the laser simulations. The bad performance of some configurations are almost guaranteed with larger values of β and augmenting $\mathbf{R_d}$ does not produce any relevant effect on the global performance of the system.

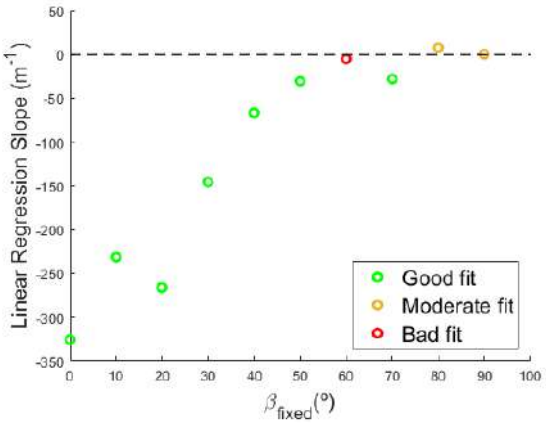

Figure 13: Linear regression for $f(\mathbf{R_d}, \beta = \beta_{fixed})$ (narrow beam pattern case)

Looking now at Figure 14 it may be concluded that, for $\beta_{fixed} \leq 40^{\circ}$, augmenting $\mathbf{R_d}$ is beneficial for the systems performance. On the opposite side, for $\beta_{fixed} \geq 50^{\circ}$, this relation reverses completely which can be seen by all positive slopes presented within this interval. This may be a result of the high probability of errors when trying to exactly locate a detected object within a wide beam pattern. These errors may cause the UAV to ignore obstacles present in their pre-planned path or route it to a unnecessary avoidance path that will bring even more risks to its mission. When $\mathbf{R_d}$ is augmented, these type of errors may be even more evident, which leads to weaker performance. Lastly, it important to remember that, when β_{fixed} is relatively small ($\leq 20^{\circ}$), the system behaves exactly like the narrow beam pattern and the laser rangefinder. Augmenting the sensor range is correlated with an

overall improvement of the systems performance.

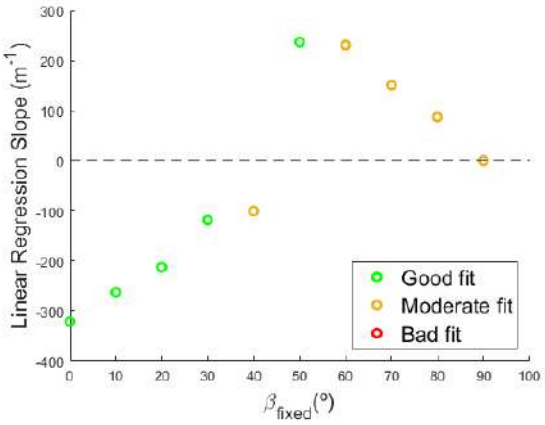

Figure 14: Linear regression for $f(\mathbf{R_d}, \beta = \beta_{fixed})$ (wide beam pattern case)

4. Hardware and Software Implementation

In order to start implementing an S&A system, it is important to do some research and select the hardware and software required for this task.

4.1. Hardware

There are basically two categories of hardware that need to be selected: Distance sensors and a Flight controller.

Two types of distance sensors were selected to perform tests afterwards: Ultrasonic sensors and laser rangefinders. The former was selected within the various MaxBotix [2] sensors in the I2CXL-MaxSonar-EZ series. The MB1242 emerged as the best option, due to its extreme noise tolerance and directional beam allied with a decent maximum range (for ultrasonic sensor standards) of 630 cm. Regarding the laser rangefinder, the LW20/C was the selected one due to its 100 m maximum range allied with a good price and reliability. Both sensors may be seen in Figure 15

(a) MB1242 (b) LW20/C

Figure 15: Selected distance sensors

In order to perform experiments with distance sensors, it is required to integrate them in a flight controller. In this subject, there are several options, all products of the Pixhawk project sponsored by Dronecode Foundation [1] members. Although, there are more recent releases of the Pixhawk series, the one chosen was the Pixhawk 2.1, now better known as the Hex Cube Black. This flight controller may be divided into three key components:

- **Pixhawk FMU (Flight Management Unit) Main Board**: The main features of this component are its 32 bit microcontroller, 256kB of RAM, 2MB of flash, an integrated accelerometer/gyro and an altimeter;
- **Vibration Damped IMU board**: Extra sensors such as accelerometer, magnetometer, gyroscope and altimeter which will reject vibrations due to its location in a vibration damped board. This extra information free of vibrations will generate redundancy on the measurements, augmenting the system overall reliability;
- **I/O ports** Includes 14 PWM servo outputs which can be used to power the vehicle motors and propellers, 2 CAN Bus interface, 2 I2C ports etc [3].

4.2. Software

After defining the devices that will be used to implement experiments, it is time to see which firmware is more adequate to pixhawk 2.1 and which Ground Control station software to use. PX4 and QGroundControl were the selected firmware software and Ground Control Station software, respectively. This was due to the great interconnection between them as they are both a DroneCode Foundation [1] project, and due to their more active user community compared to their "rivals": Ardupilot and Mission Planner.

5. Sensor Experiments

5.1. Bench Tests

Even though, there are proper data sheets [11] [5] for each one of the sensors used, it is prudent to perform various experiments to obtain real limitations in terms of ranging and field of view for the selected devices. Hereupon, the idea with these experiments is to determine the sensors detection rates and the precision/accuracy of their measurements. These data will be collected for various distances and angles.

5.1.1 Ultrasonic Sensor

Figure 16(a) demonstrates an experiment where the object to detect is in front of the sensor. In Figure 16, the idea is to determine the sonar capability of detecting an object which has an angular deflection (θ) in relation to the sensor. In both cases, the target object is a square wooden board with a 46 cm side and 2 cm thick as seem in Figure 16(c).

This board is always perpendicular to the blue line, which represents the minimal distance between the sonar and the object. During these experiments, the board was positioned at several distances from the Sonar (20 cm to 760 cm) and kept at each position for 30 seconds. The idea with this approach was to obtain, for each position, the fraction of time where the sensor was actually detecting its target and how much these measurements were deviated from the correct distance.

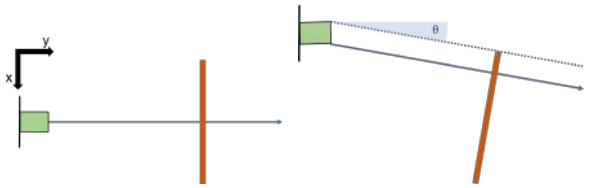

(a) Straight on obstacle (b) Off-set obstacle

(c) Experimental setup

Figure 16: Ultrasonic sensor bench test

Before proceeding to the results presentation, there are some considerations to take into account first. Due to the fact that these results were obtained with a statistical approach, a minimum detection rate was set at (100%) given the high risk associated with S&A missions. Furthermore, it is important to take into account that the target material could affect the performance of this sensor. In [10] it is mentioned that this sensor's ideal surface to detect is hard, smooth and non-porous. Although wood is not a perfect example of an ideal surface, its properties are not far from that category. The last important aspect to refer is the fact that a targets rotation within its inertial referential affects this sensor performance. The sonar can only detect a target if the emitted sound is reflected back. Following the sound reflection laws this can only be possible if the normal vector of the surface in question is aligned with the emitted sound trajectory until it reaches the target.

Following the logic explained previously, the sonar was tested and the key results can be observed in the next figures.

Figure 17 shows the sensor's detection rate for various distances and orientations. As expected, the sensor performed better when the obstacle was completely in front of it, achieving a maximum range of 660 cm (slightly better than the 630 cm stated in the data sheet). Additionally, the maximum range decreased when augmenting θ, which was also an expected behaviour.

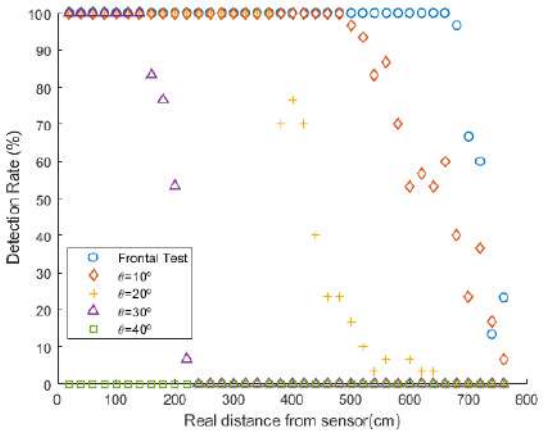

Figure 17: MB1242 detection rate from several distances and orientations

Moreover, this sensor proved to be very directional as it stopped detecting any targets at $\theta = 40°$. Using each maximum range obtained for its corresponding orientation of the obstacle, an experimental beam pattern was drawn as seen in Figure 18. Beam patterns like this, can be extremely useful for sense and avoidance missions, as they limit their detection volume to a well determined direction, so the device that is controlling it knows with a considerable precision in which direction the target is located.

Finally, the average absolute error registered never surpassed 4 cm, which is a really good margin of error.

To sum up, this sensor capabilities were found to match the expectations, mixing a narrow beam pattern with a maximum range above 6 m.

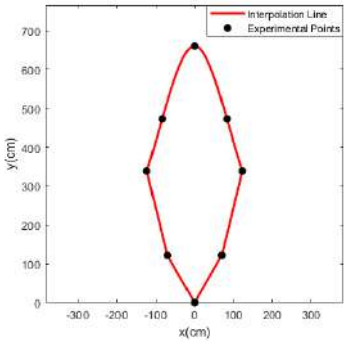

Figure 18: MB1242 experimental beam pattern

5.1.2 Laser Rangefinder

For this purpose, an identical experiment to the one used for sonar was implemented but only with a frontal test as the laser rangefinder is completely directional.

Figure 19 shows that the laser kept a perfect detection rate until 85 m. Beyond this distance, it started failing and the 100 m mark stated in the data sheet, and represented as a dashed red line was the last distance that the laser managed to detect, even though it was already with a poor detection rate (less than 30%). Although the full range promised in the data sheet was not obtained with a perfect detection rate, this 85 m mark obtained during this experiment is more than enough to optimize a Sense and Avoidance system that uses a Laser Rangefinder.

Regarding accuracy, LW20/C managed to keep an average absolute error between 0 cm and 25 cm which is quite satisfactory taking into account the considerable distances that this type of sensor can measure.

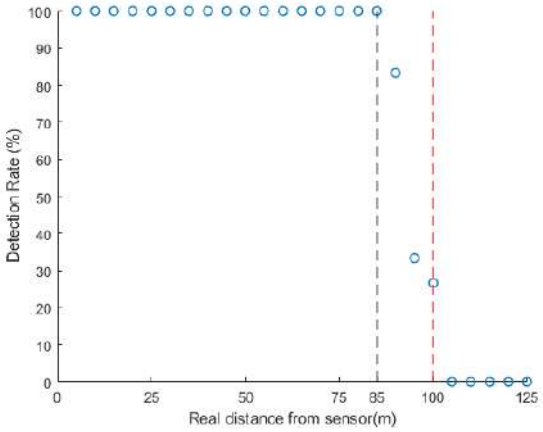

Figure 19: LW20/C detection rate from several distances

5.2. Rover Experiments

The idea is to put the rover travelling along a rectilinear trajectory with a distance sensor pointing forward and an obstacle in the middle of its path. If the avoidance algorithm is active, it will try to stop at a certain point depending on the safety margin given as input. In order to test this tool, the rover was taken to the field as seen in Figure 20. The parameter that controls the safety margin (Avoid_Margin) was incremented by one meter until it reached its maximum value of 10 m. For each value of Avoid_Margin, both reported and real stop distances were registered. Figure **??** shows precisely this information when the rover was equipped with the laser rangefinder and the ultrasonic sensor.

(a) On bench (b) In testing

Figure 20: Final rover configuration

Through the analysis of Figures 21 and 22, it is clear the inability of the rover to stop before the safety margin defined by the Avoid_Margin parameter regardless of the sensor used, however, the rover has indeed reacted to the presence of the obstacle and was able to effectively stop which can still be seen as a success even more so considering that the rover never exceeded in more than one meter the stipulated point for its stop as seen by all the dots in both graphics above the dashed line.

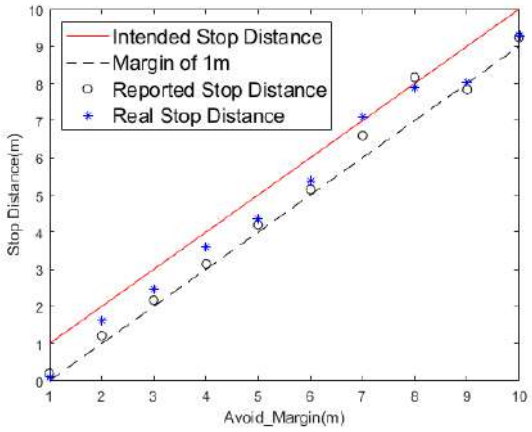

Figure 21: Simple avoidance results with laser

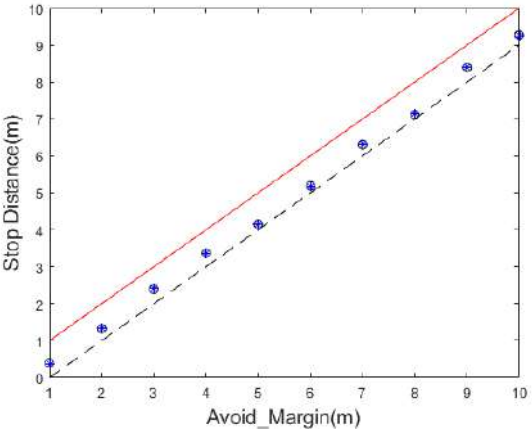

Figure 22: Simple avoidance results with sonar

6. Conclusions

The initial idea for this thesis was to deepen a previously initiated study on Sense and Avoidance systems for small fixed wing UAVs with special focus on the detection phase. After a brief introduction and the consequent delimitation of the objectives for this thesis, we proceeded with an analysis about sense and avoidance systems, listing the various types of sensors that can be used, underlining the most appropriate for this specific problem and, finally, presenting various types of avoidance algorithms with special focus on the Potential Fields Method that was already implemented and would be used in the future.

This was followed by a simulation phase where it was concluded that augmenting both ultrasonic sensors or laser rangefinders range will produce positive effects on the systems performance, however, it is not the preponderant parameter. The sensor's orientation proved to be the variable with a more well defined minimum. Additionally, it was also concluded that a bad orientation can solely define the systems outcome, making the maximum range influence disappear.

Next, it was concluded that the best approach for this problem would be to use the Lightware LW20/C as laser rangefinder, Maxbotix MB1242 as the ultrasonic sensor and the pixhawk 2 (or cube black) as flight controller. Concerning software, the two best known options for controller firmware and ground control station software were presented and the final decision was to choose px4 and QGroundControl respectively as they offer the most active user development community.

Finally, it was concluded that the laser rangefinder maximum range is slightly less than what was stated in the data sheet (-15%) and ultrasonic sensor was actually above the expectations by almost 5%. The ultrasonic sensor experimental beam pattern proved to be extremely directional confirming the data sheet information. Regarding, the sensor's measurement errors, it was concluded that this would not be a problem in the future as neither one of them passed 0.7% of their maximum range. Regarding the rover tests, it was concluded that the system was able to react to the presence of obstacles, however, its reaction was not ideal as it never managed to stop before the established safety margin. This error is believed to be directed related to a bad calibration.

References

[1] Dronecode foundation. URL:https://www.dronecode.org/.

[2] Maxbotix. URL:https://www.maxbotix.com/.

[3] Pixhawk v2 feature overview. URL:https://hexadrone.fr/img/cms/DRS_Pixhawk-2.pdf.

[4] Tekever ar4. URL:http://uas.tekever.com/ar4-evo/.

[5] I2cxl-maxsonar-ez series data sheet, 2012.

[6] N. Alturas. Modeling and optimization of an obstacle detection system for small uav's. Master's thesis, IST, January 2021.

[7] J. Alves. Path planning and collision avoidance algorithms for small rpas. Master's thesis, IST, June 2017.

[8] A. A. . A. M. . P. O. . E. Badreddin. A comparative study of collision avoidance techniques for unmanned aerial vehicles. *IEEE International Conference on Systems*, 2013.

[9] C. Barroso. Firefront: an inteligent system that will help detect and fight forest fires. Technical report, Lusa, July 2020. URL:https://tecnico.ulisboa.pt/en/news/firefront-an-intelligent-system-that-will-help-detect-and-fight-forest-fires/.

[10] R. Burnett. Frequently asked questions about ultrasonic sensors.

[11] R. Burnett. Lw20 lidar sensor datasheet.

[12] K. Dalamagkidis. Classification of uavs. pages 83–91, 2015. in Handbook of Unmanned Aerial Vehicles, doi:10.1007/978-90-481-9707-1_94.

[13] P. Finnegan. 2020/2021 world civil unmanned aerial systems. Technical report, Teal Group, 2020.

[14] J. F. Keane and S. S. Carr. A brief history of early unmanned aircraft. *Johns Hopkins APL Technical Digest (Applied Physics Laboratory)*, 32(3):558–571, 2013.

[15] X.Yu and Y.Zhang. Sense and avoid technologies with applications to unmanned aircraft systems: Review and prospects. *Progress in Aerospace Sciences*, 2015. https://doi.org/10.1016/j.paerosci.2015.01.001.